Supporting Information for:

Electroluminescence and Fluorescence Response towards Acid Vapors Depending on the Structures of Indole-fused Phospholes

Peng Gong[a], Kaiqi Ye[a,*], Jingbo Sun[a], Peng Chen[b], Pengchong Xue[a], Hao Yang[a] and Ran Lu[a,*]

[a] State Key Laboratory of Supramolecular Structure and Materials, College of Chemistry, Jilin University, Changchun 130012, P. R. China

[b] Key Laboratory of Functional Inorganic Material Chemistry (MOE), School of Chemistry and Materials Science, Heilong-jiang University, No. 74, Xuefu Road, Nangang District, Harbin, P. R. China

E-mail: luran@mail.jlu.edu.cn

Table S1 Photophysical data of **2-DIPO** and **3-DIPO**.

Compound	Solution [a]				Solid [c]	
	λ^{abs}_{max} (nm)	E ($L \cdot mol^{-1} \cdot cm^{-1}$)	λ_{em} (nm)	Φ_F [b]	λ_{em} (nm)	Φ_F
2-DIPO	261, 279, 316, 331, 409	4×10^4, 2.2×10^4, 1.3×10^4, 1×10^4, 1.2×10^4	494	0.70	530	0.53
3-DIPO	265, 317, 430	3.5×10^3, 7.6×10^2, 11	548	0.02	574	0.13

[a] in THF (5 μM); [b] Using 9,10-diphenylanthracene in benzene (Φ_F = 85 %) as the standard; [c] solid state.

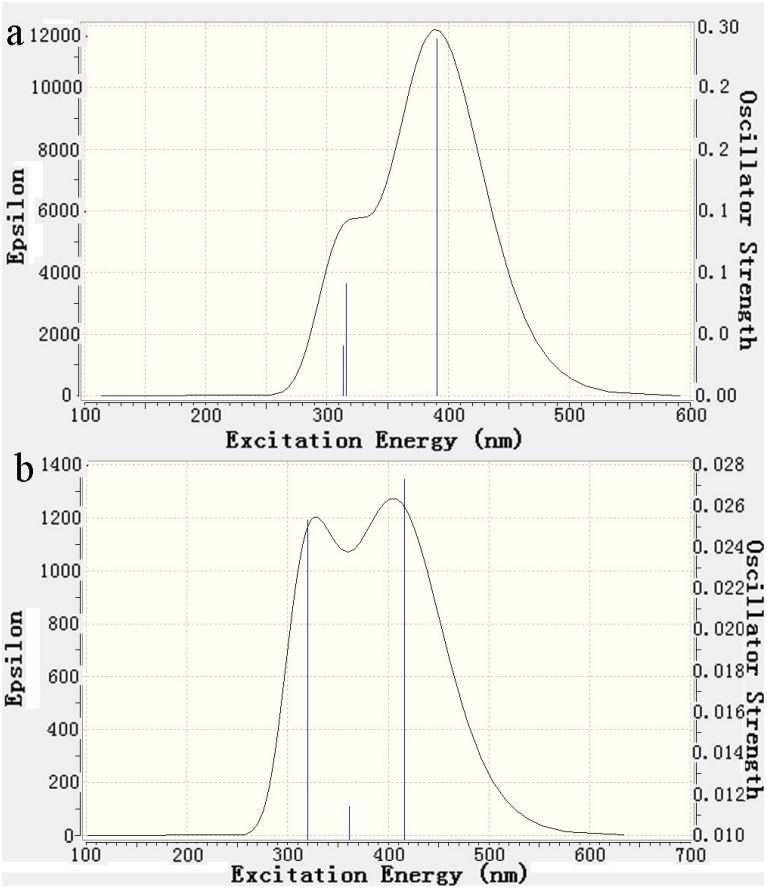

Figure S1 UV-vis absorption spectra of **2-DIPO** (a) and **3-DIPO** (b) based on TD-DFT calculation.

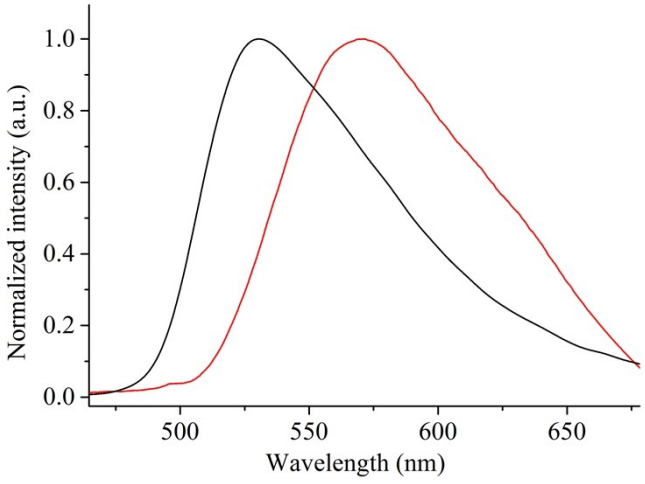

Figure S2 Normalized fluorescence emission spectra of **2-DIPO** (black) and **3-DIPO** (red) in solid states (λ_{ex} = 410 nm).

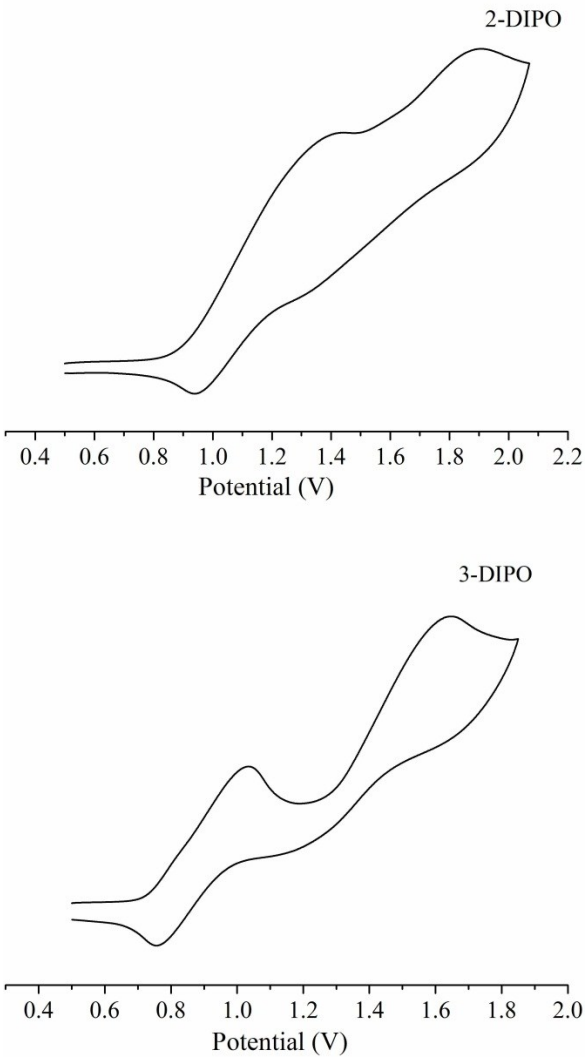

Figure S3 Cyclic voltammetry diagrams of **2-DIPO** and **3-DIPO** in anhydrous CH_2Cl_2 with 0.1 M Bu_4NBF_4 as electrolyte at a scan rate of 50 $mV \cdot s^{-1}$.

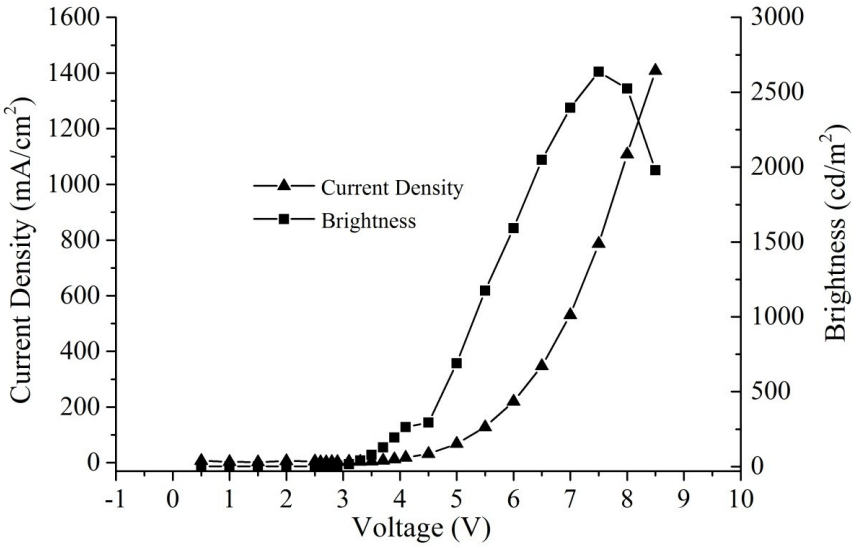

Figure S4 J–V–L characteristics of device A.

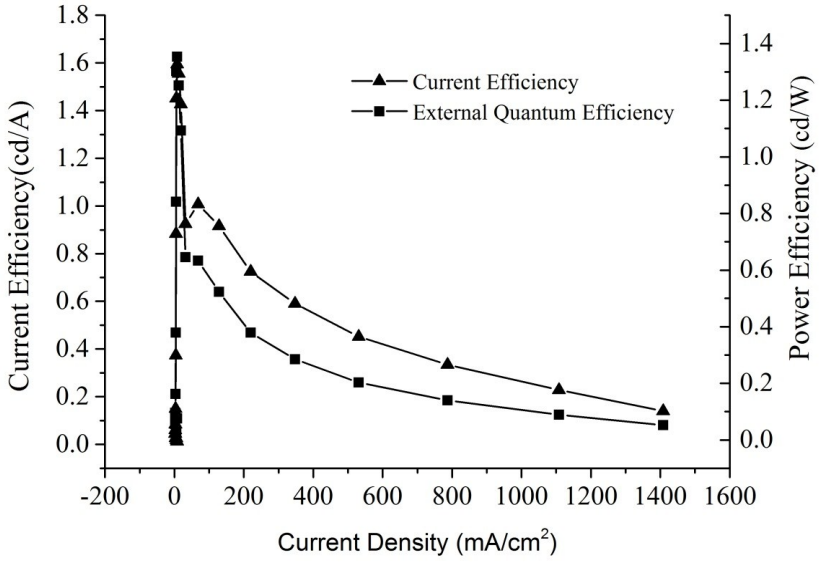

Figure S5 Current efficiency and power efficiency–current density of device A.

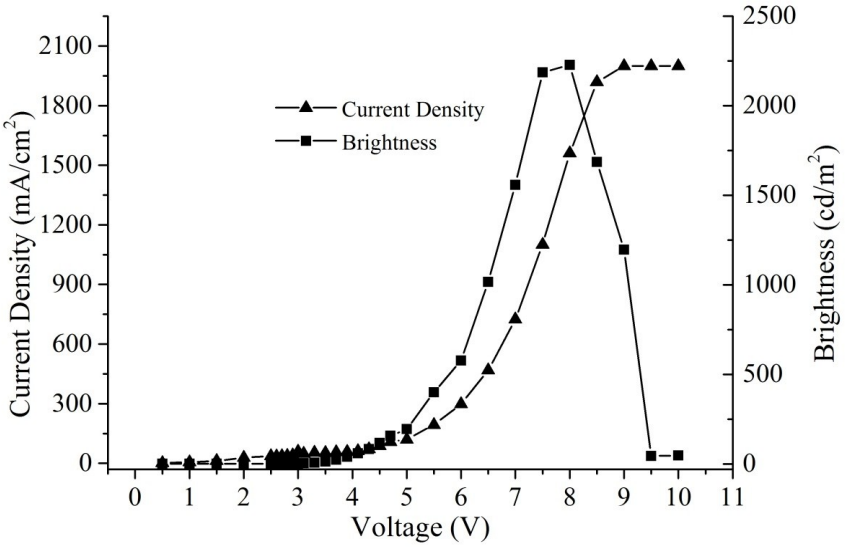

Figure S6 J–V–L characteristics of device B.

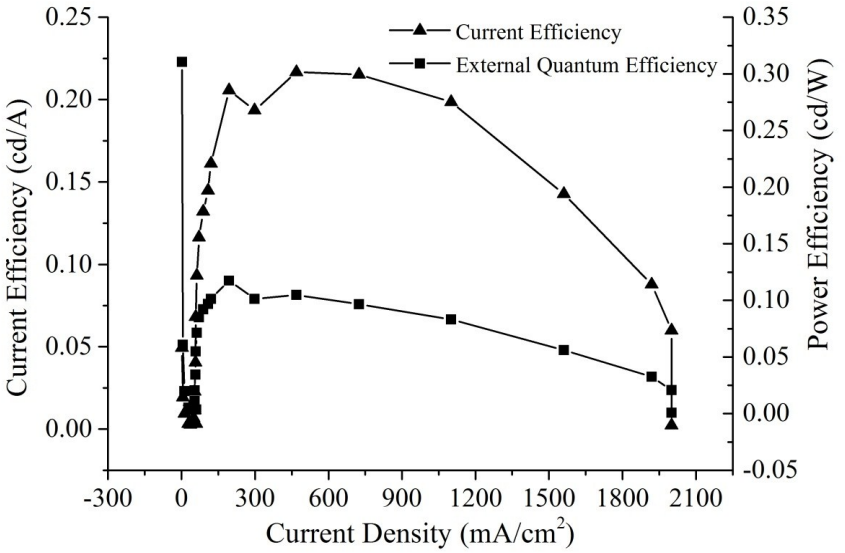

Figure S7 Current efficiency and power efficiency–current density of device B.

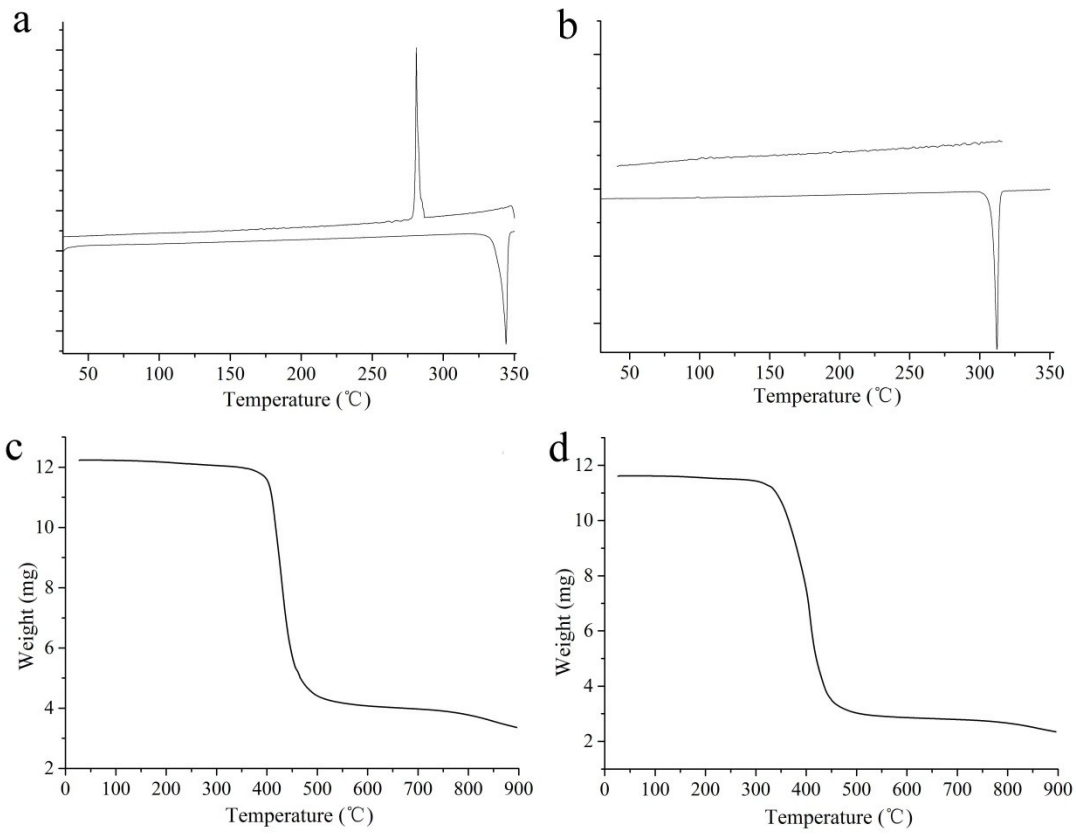

Figure S8 DSC thermograms of **2-DIPO** (a) and **3-DIPO** (b); TGA thermograms of **2-DIPO** (c) and **3-DIPO** (d) under a nitrogen atmosphere at a heating/cooling rate of 10 °C min^{-1}.

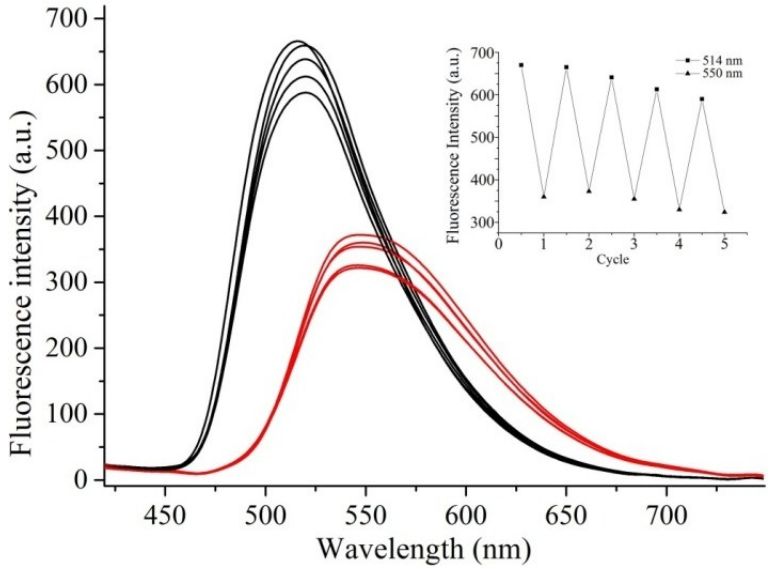

Figure S9 The fluorescence spectral changes of **2-DIPO** in filter paper strip upon exposed to HCl (red) and NH_3 vapors (black). Inset: the reversibility in the sensory processes (λ_{ex} = 365 nm).

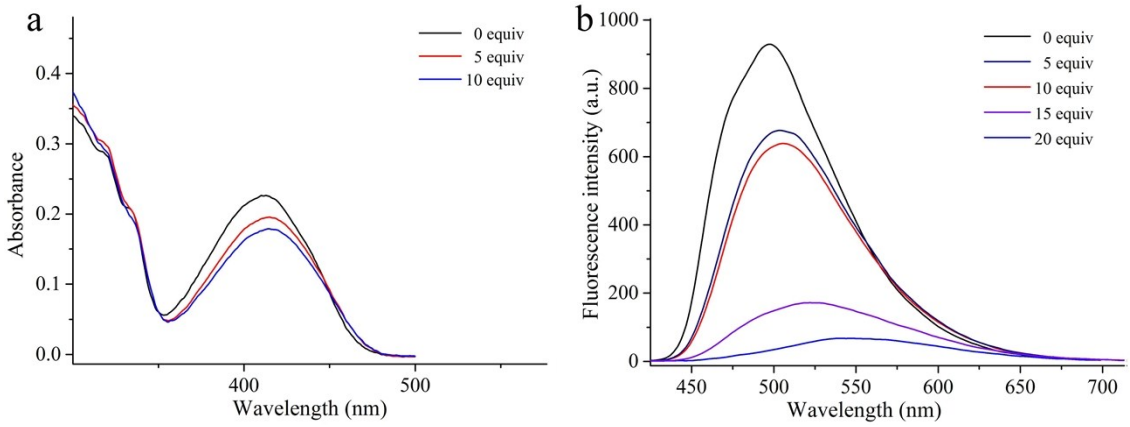

Figure S10 UV-vis absorption (a) and fluorescence emission (b, λ_{ex} = 390 nm) spectra of **2-DIPO** in toluene (5.0×10^{-6} M) upon the addition of different amount of trifluoromethanesulfonic acid.

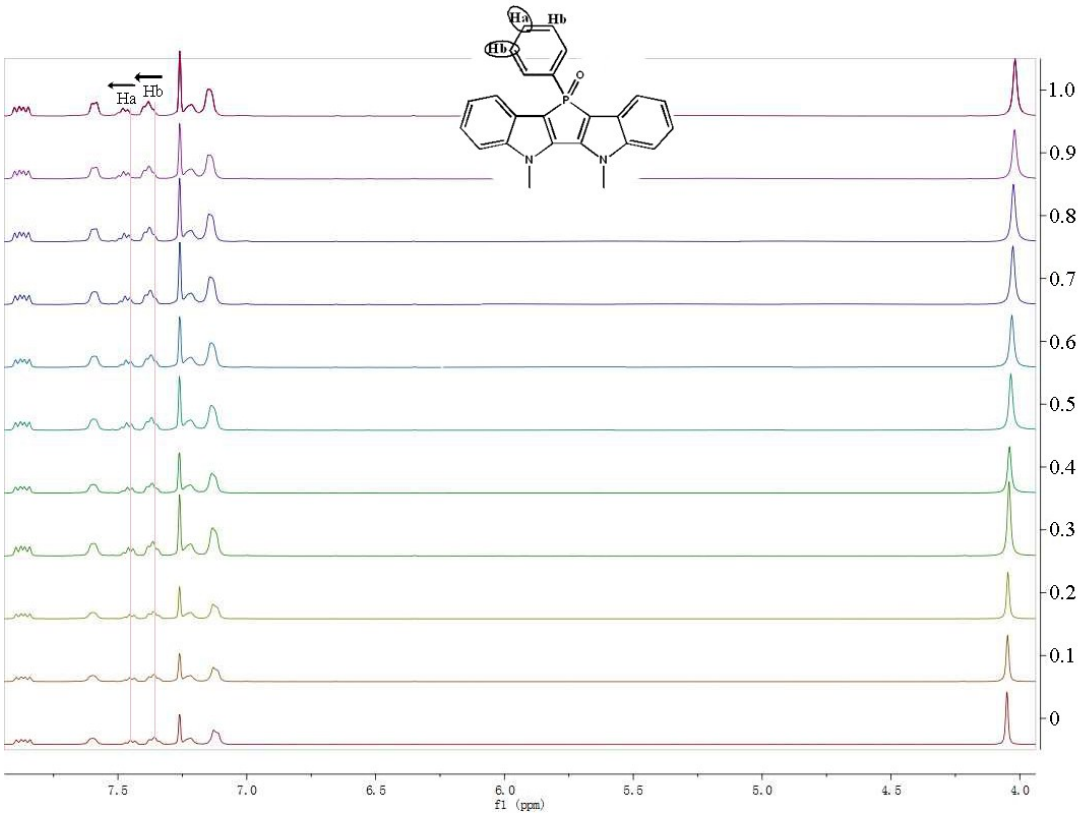

Figure S11 ^{1}H NMR spectra (400 MHz) of **2-DIPO** in $CDCl_3$ upon the addition of different amount of trifluoroacetic acid (from 0.1 equiv. to 1.0 equiv.).

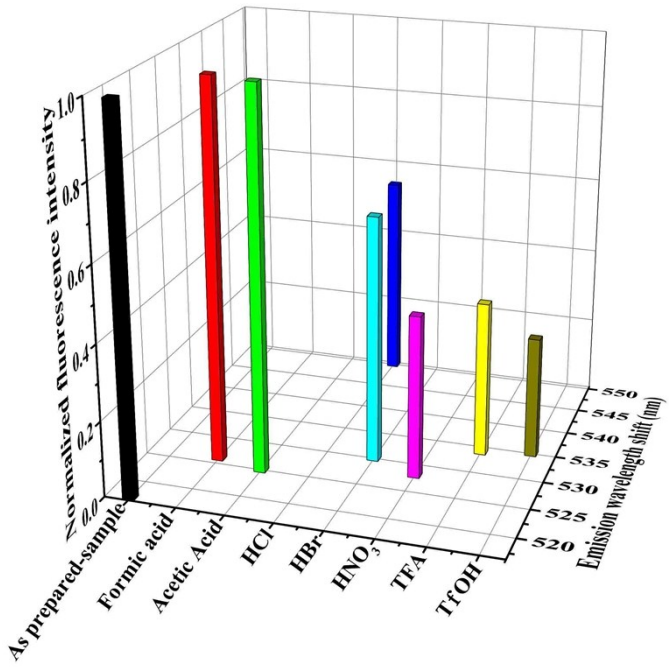

Figure S12 The emission intensity at maximal emission wavelength of **2-DIPO** in test paper upon exposed to different acid vapors (λ_{ex} = 365 nm).

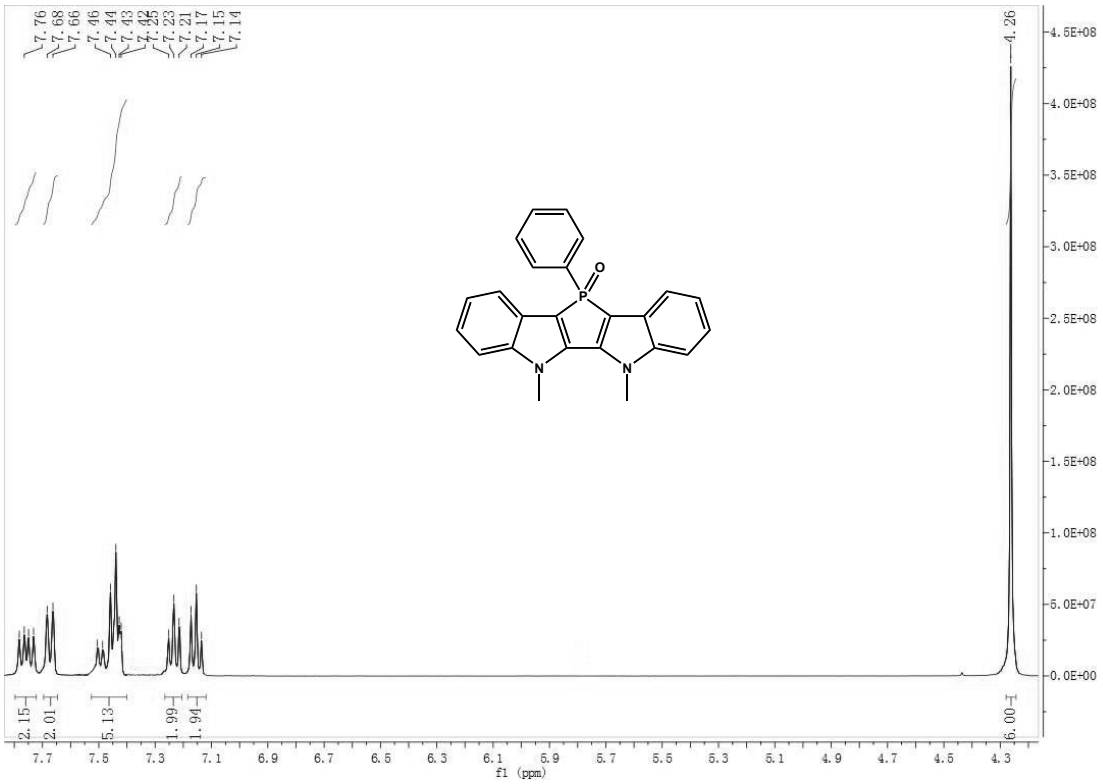

Figure S13 ^{1}H NMR (400 MHz, DMSO-d_6) spectrum of **2-DIPO**.

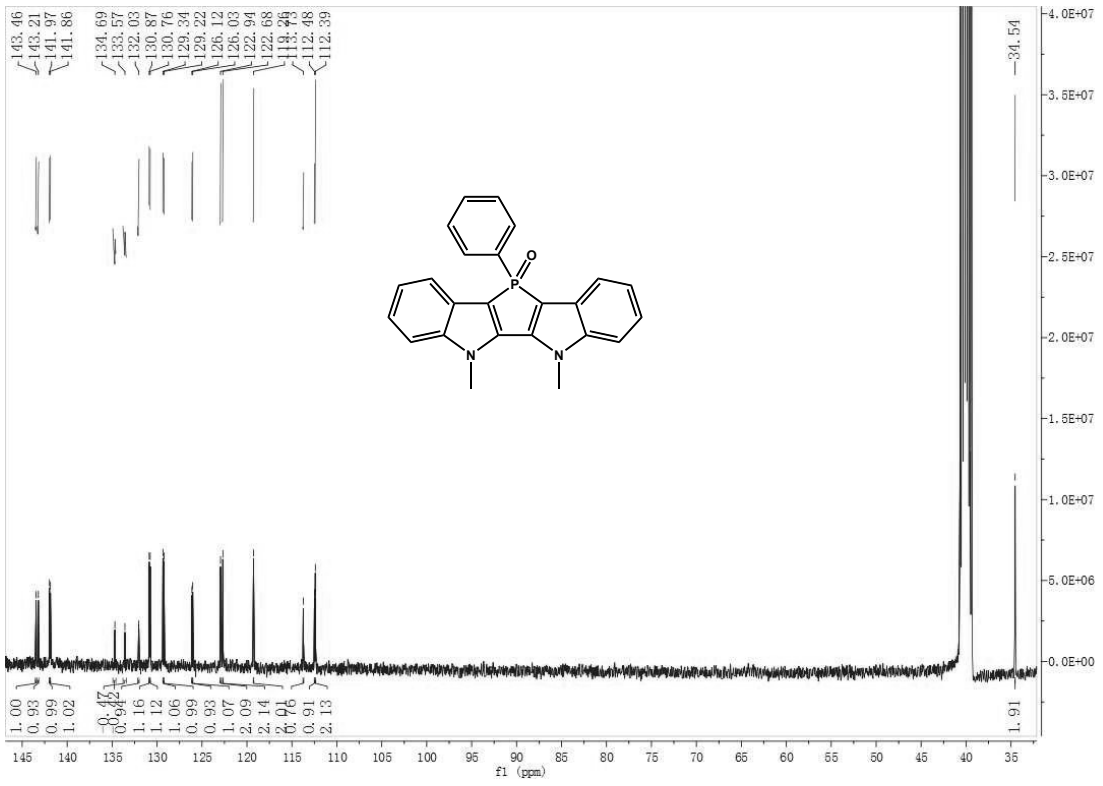

Figure S14 Quantitative ^{13}C NMR (100 MHz, DMSO-d_6) spectrum of **2-DIPO**.

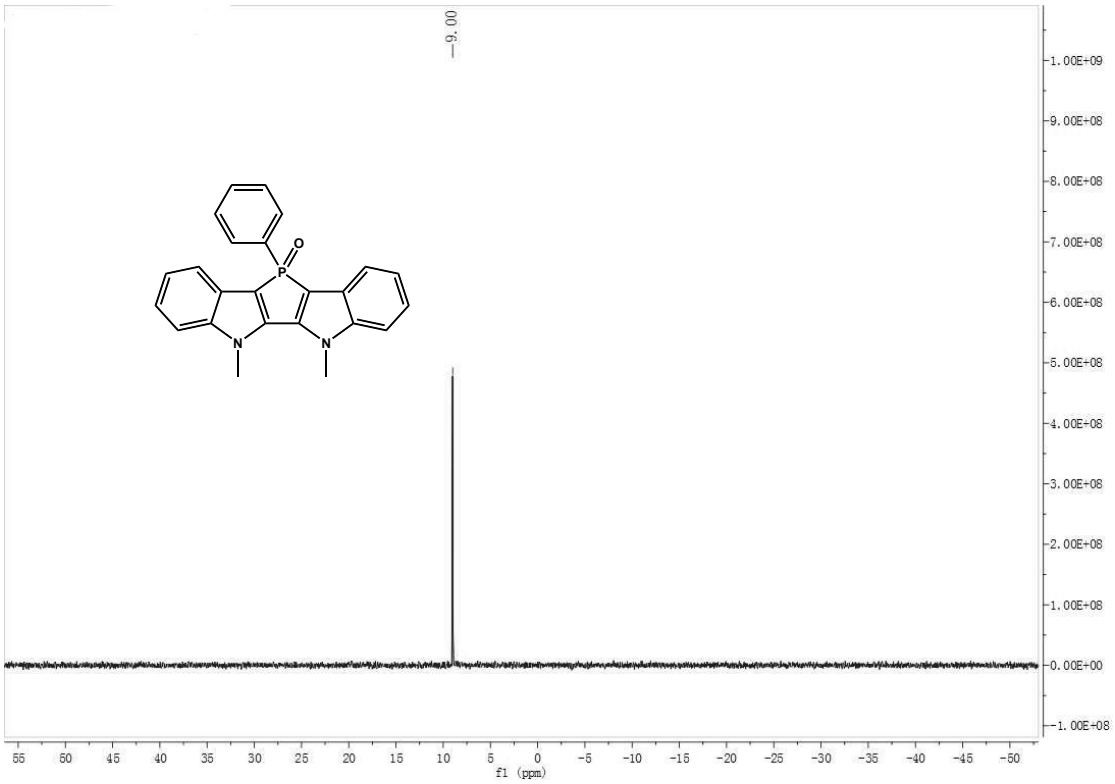

Figure S15 ^{31}P NMR (162 MHz, DMSO-d_6) spectrum of **2-DIPO**.

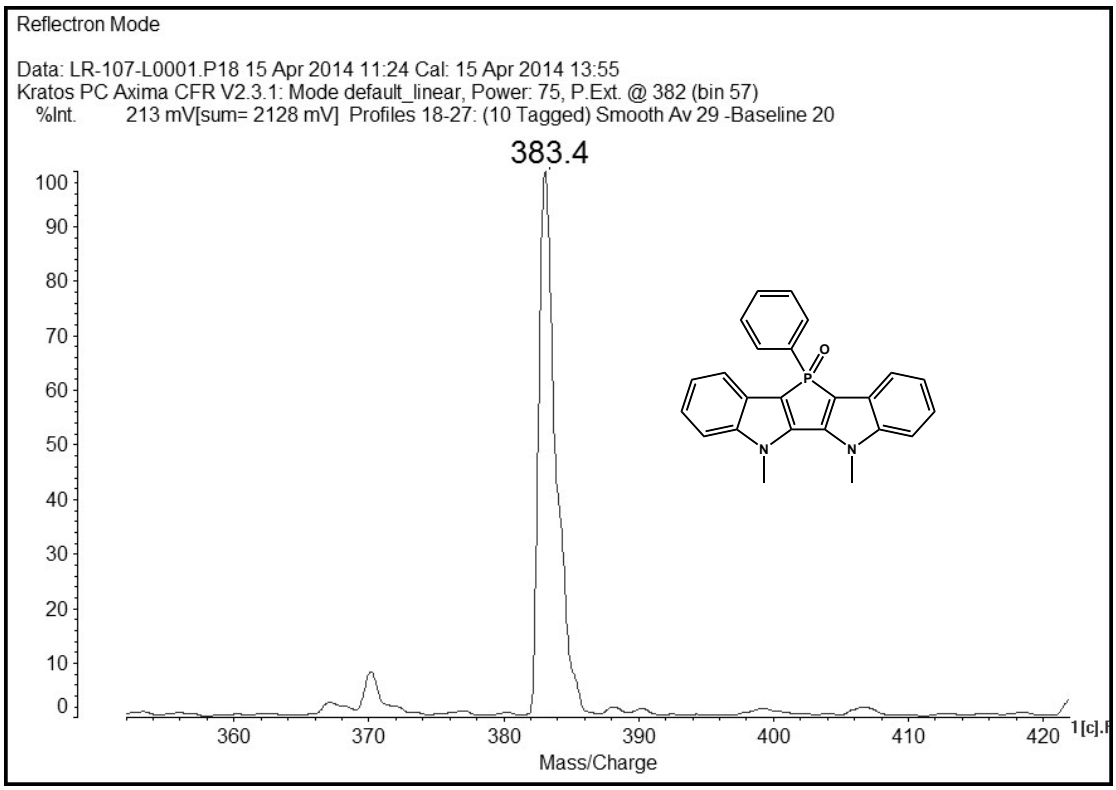

Figure S16 MALDI/TOF MS spectrum of **2-DIPO**.

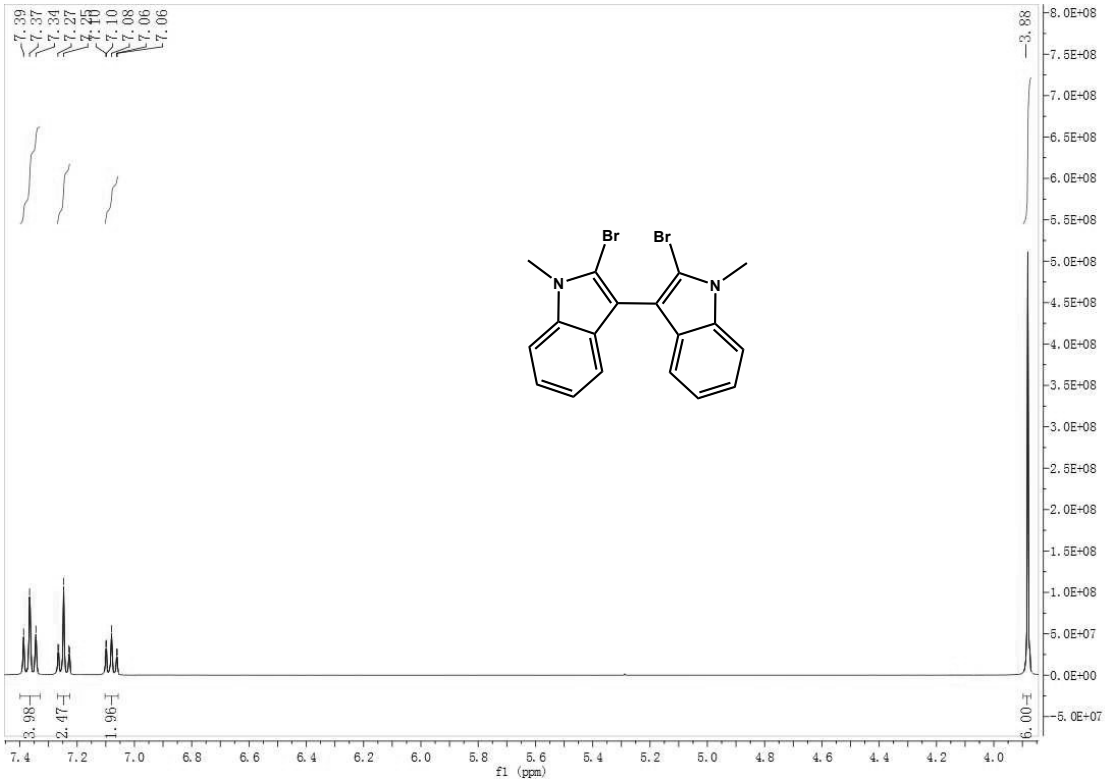

Figure S17 ^{1}H NMR (400 MHz, $CDCl_3$) spectrum of **3**.

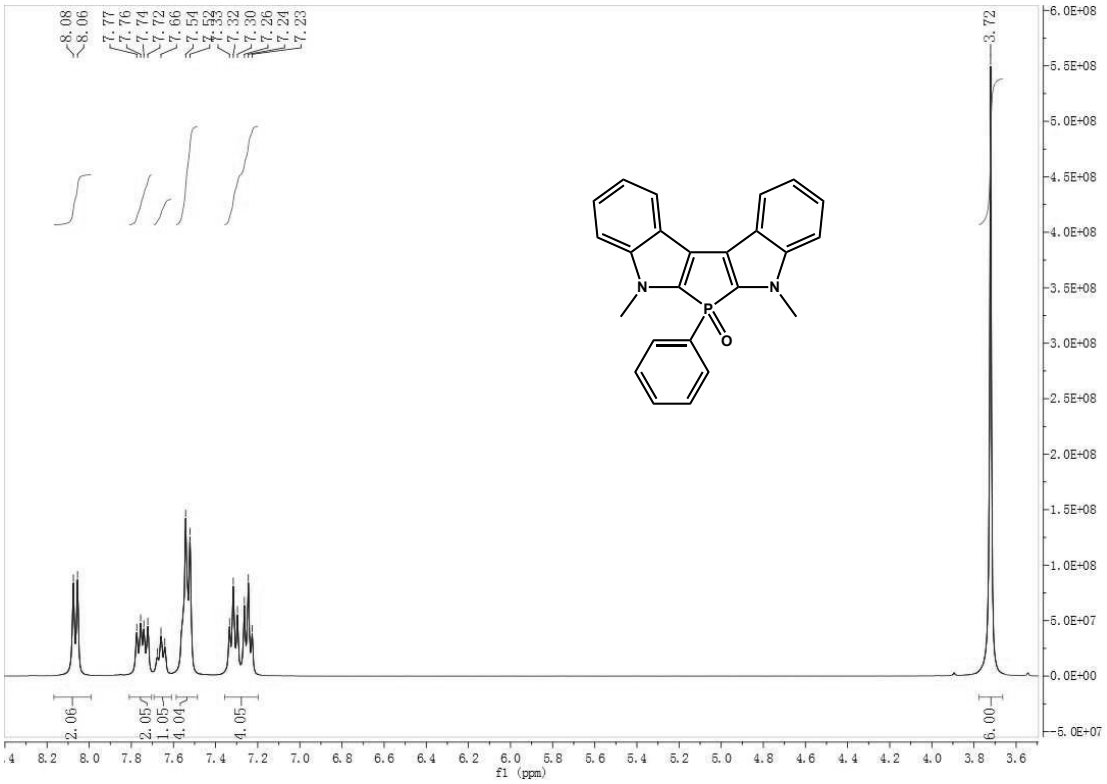

Figure S18 ^{1}H NMR (400 MHz, DMSO-d_6) spectrum of **3-DIPO**.

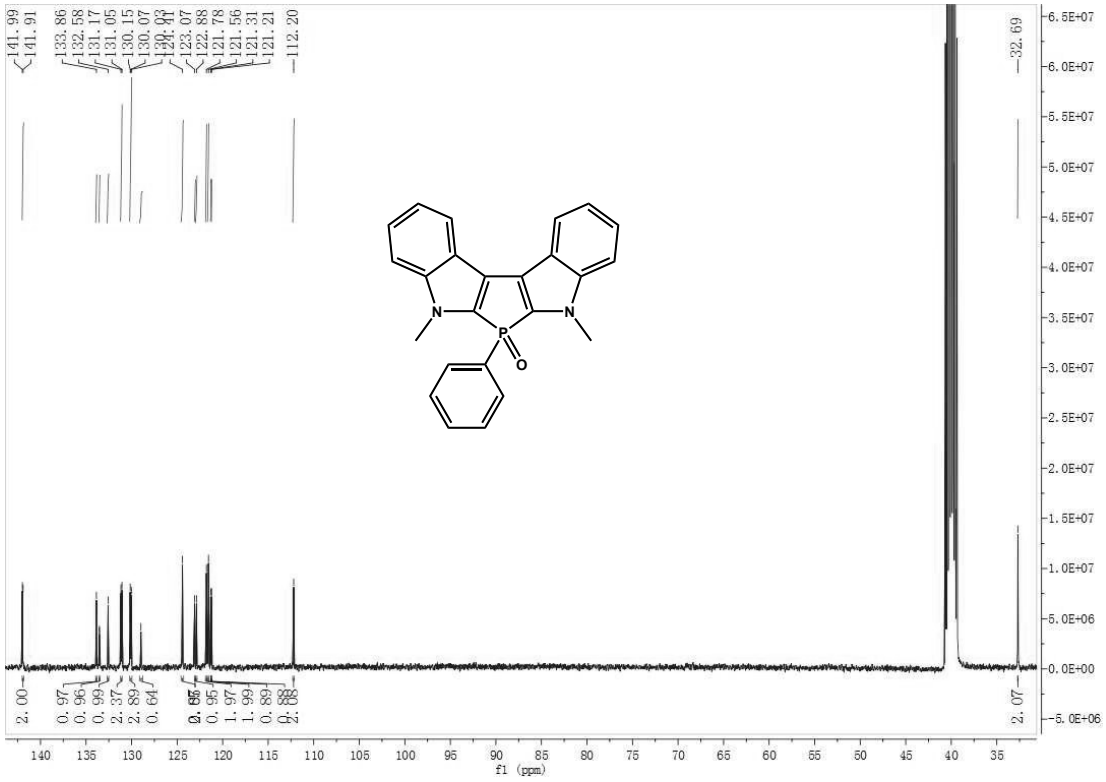

Figure S19 Quantitative ^{13}C NMR (100 MHz, DMSO-d_6) spectrum of **3-DIPO**.

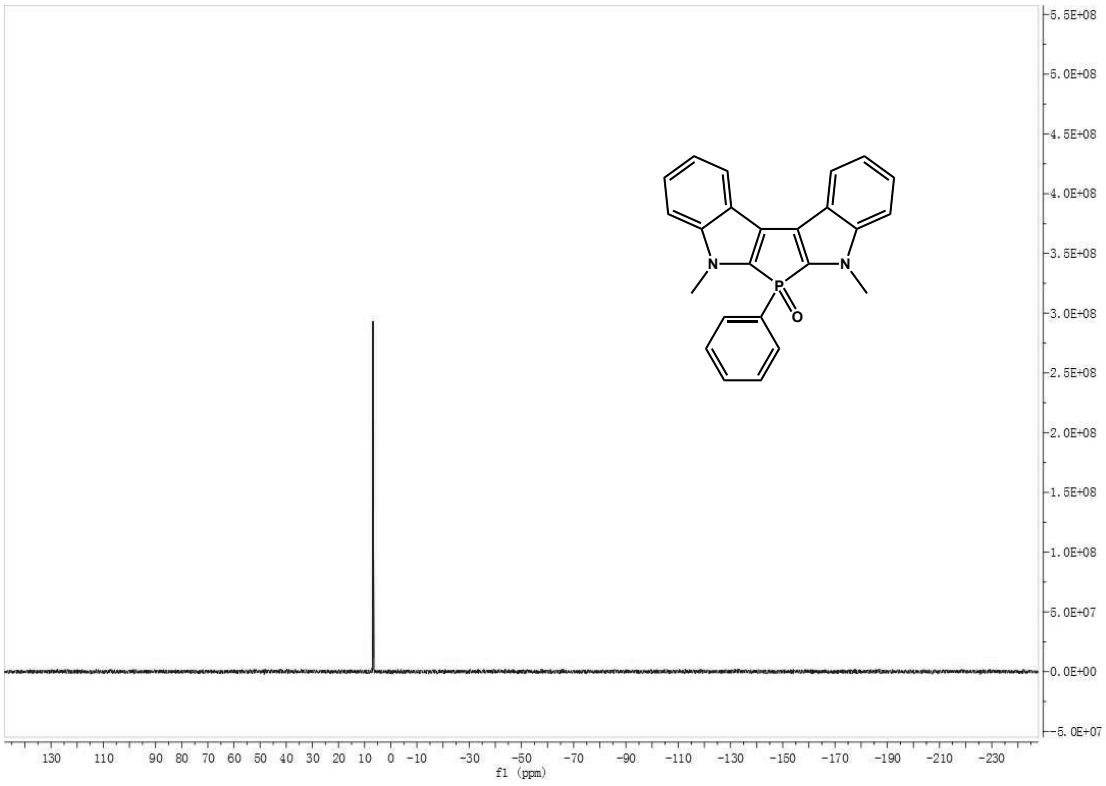

Figure S20 ^{31}P NMR (162 MHz, DMSO-d_6) spectrum of **3-DIPO**.

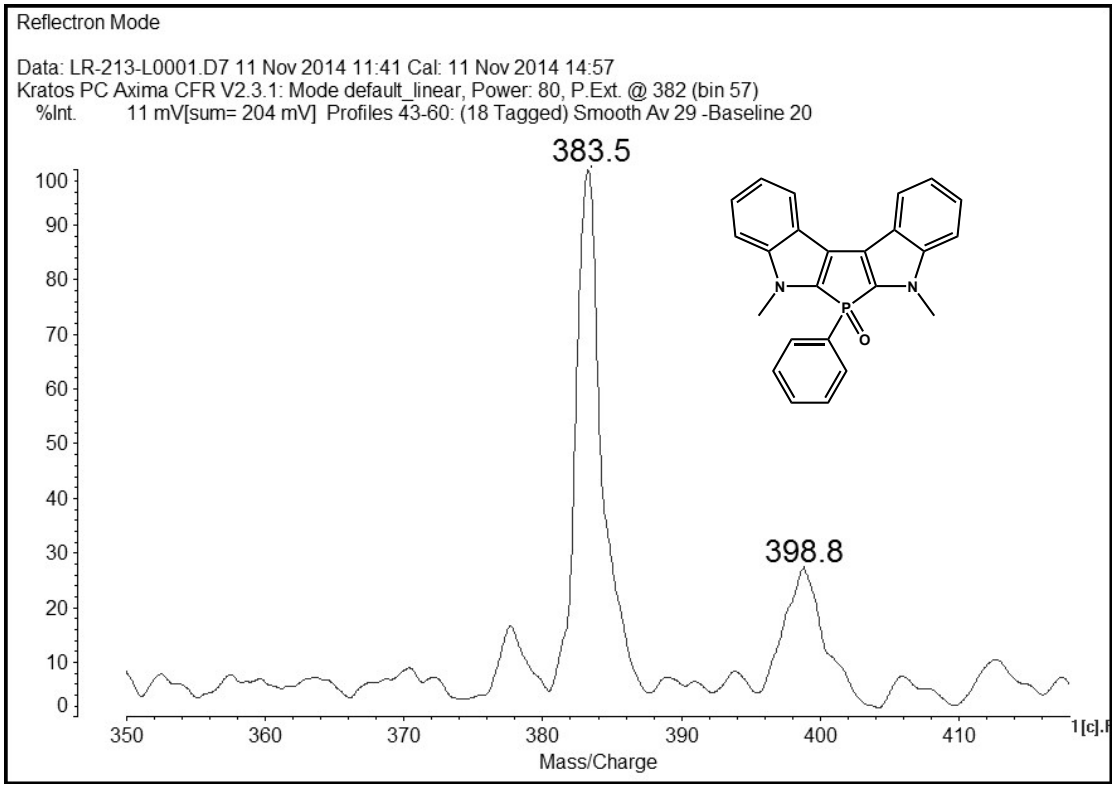

Figure S21 MALDI/TOF MS spectrum of **3-DIPO**.